NRC·CNRC

NRC Publications Archive
Archives des publications du CNRC

Comparative study of microlaser excitation thermography and microultrasonic excitation thermography on submillimeter porosity in carbon fiber reinforced polymer composites

Zhang, Hai; Fernandes, Henrique; Hassler, Ulf; Ibarra-castanedo, Clemente; Genest, Marc; Robitaille, François; Joncas, Simon; Maldague, Xavier

This publication could be one of several versions: author's original, accepted manuscript or the publisher's version. / La version de cette publication peut être l'une des suivantes : la version prépublication de l'auteur, la version acceptée du manuscrit ou la version de l'éditeur.
For the publisher's version, please access the DOI link below./ Pour consulter la version de l'éditeur, utilisez le lien DOI ci-dessous.

Publisher's version / Version de l'éditeur:
https://doi.org/10.1117/1.OE.56.4.041304
Optical Engineering, 56, 4, 2016-09-30

NRC Publications Record / Notice d'Archives des publications de CNRC:
https://nrc-publications.canada.ca/eng/view/object/?id=3e9217c6-0dc9-4105-9349-8201cbba6d0b
https://publications-cnrc.canada.ca/fra/voir/objet/?id=3e9217c6-0dc9-4105-9349-8201cbba6d0b

Access and use of this website and the material on it are subject to the Terms and Conditions set forth at https://nrc-publications.canada.ca/eng/copyright
READ THESE TERMS AND CONDITIONS CAREFULLY BEFORE USING THIS WEBSITE.

L'accès à ce site Web et l'utilisation de son contenu sont assujettis aux conditions présentées dans le site https://publications-cnrc.canada.ca/fra/droits
LISEZ CES CONDITIONS ATTENTIVEMENT AVANT D'UTILISER CE SITE WEB.

Questions? Contact the NRC Publications Archive team at PublicationsArchive-ArchivesPublications@nrc-cnrc.gc.ca. If you wish to email the authors directly, please see the first page of the publication for their contact information.

Vous avez des questions? Nous pouvons vous aider. Pour communiquer directement avec un auteur, consultez la première page de la revue dans laquelle son article a été publié afin de trouver ses coordonnées. Si vous n'arrivez pas à les repérer, communiquez avec nous à PublicationsArchive-ArchivesPublications@nrc-cnrc.gc.ca.

National Research Council Canada | Conseil national de recherches Canada

Canada

Comparative study of microlaser excitation thermography and microultrasonic excitation thermography on submillimeter porosity in carbon fiber reinforced polymer composites

Hai Zhang,[a,*] Henrique Fernandes,[a,b] Ulf Hassler,[c] Clemente Ibarra-Castanedo,[a] Marc Genest,[d] François Robitaille,[e] Simon Joncas,[f] and Xavier Maldague[a]
[a]Laval University, Department of Electrical and Computer Engineering, Computer Vision and Systems Laboratory, 1065 Avenue de la Médecine, Quebec G1V 0A6, Canada
[b]Federal University of Uberlandia, Department of Mechanical Engineering, 2121 Avenida Joao Naves de Avila, Uberlandia 38400-902, Brazil
[c]Fraunhofer Development Center X-ray Technologies (EZRT), Department of Application Specific Methods and Systems, Fraunhofer IIS, Flugplatzstrasse 75, 90768 Fuerth, Germany
[d]National Research Council Canada, Aerospace Portfolio, Structures, Materials and Manufacturing, 1200 Montreal Road, Ottawa K1A 0R6, Canada
[e]University of Ottawa, Department of Mechanical Engineering, 161 Louis Pasteur, Ottawa K1N 6N5, Canada
[f]École de Technologie Supérieure, Department of Automated Manufacturing Engineering, 1100 rue Notre-Dame Ouest, Montreal H3C 1K3, Canada

Abstract. Stitching is used to reduce incomplete infusion of T-joint core (dry-core) and reinforce T-joint structure. However, it may cause new types of flaws, especially submillimeter flaws. Thermographic approaches including microvibrothermography, microlaser line thermography, and microlaser spot thermography on the basis of pulsed and lock-in techniques were proposed. These techniques are used to detect the submillimeter porosities in a stitched T-joint carbon fiber reinforced polymer composite specimen. X-ray microcomputed tomography was used to validate the thermographic results. Finally an experimental comparison of microlaser excitation thermography and microultrasonic excitation thermography was conducted. *© 2016 Society of Photo-Optical Instrumentation Engineers (SPIE)* [DOI: 10.1117/1.OE.56.4.041304]

Keywords: laser line thermography; laser spot thermography; vibrothermography; x-ray computed tomography; composite.

Paper 160680SSP received May 3, 2016; accepted for publication Aug. 9, 2016; published online Sep. 30, 2016.

1 Introduction

Stitching is used to reduce incomplete infusion of T-joint core (dry-core) and reinforce T-joint structure in carbon fiber reinforced polymer composites (CFRP).[1] However, it may cause new types of flaws, especially submillimeter flaws.[2,3] Microscopic inspection is the most often used technique for identifying the submillimeter flaws, but it is time-consuming and destructive.[2,3] Therefore, nondestructive testing (NDT) of materials is significant and increasingly used nowadays.[4,5] NDT of composite materials is complicated due to the wide range of flaws encountered (including delamination, microcracking, fiber fracture, fiber pull-out, matrix cracking, inclusions, voids, and impact damage). The ability to quantitatively characterize the type, geometry, and orientation of flaws is essential.[6] Ultrasonic C-scan (UT) is the most often used NDT technique for composites. UT has significant advantages on large-sized defects such as delamination, but it cannot detect microsized defects in composites.[2,3] Infrared thermography (IRT) is becoming increasingly popular in the recent years as an NDT technique due to its fast inspection rate, contact-less, spatial resolution, and acquisition rate improvements of infrared cameras as well as the development of advanced image processing techniques. IRT was already used for diagnostics and monitoring in several fields such as thermal comfort,[7] buildings,[8,9] cultural heritage,[10] artworks,[11–15] composite materials,[16,17] and so on.[18–21]

The most often used IRT techniques are pulsed thermography and lock-in thermography, which use high-energy lamps to produce a uniform heating source on the specimen surface. The heat transmits through the specimen to the subsurface anomalies such as defects or damages and then returns to the specimen surface. When the pulsed heat flux is delivered to the specimen surface, an out-of-plane heat flow is produced in the specimen. A uniform temperature rise will be recorded if there are no defects in the specimen. If there are defects, such as voids or delamination, a localized high-temperature zone will be observed above the defect due to the insulation effect. The shape of the high-temperature zone represents the defect shape. The location, shape, and size of the defect can be estimated from the temperature distribution on the sample surface.[22,23] The classical optical excitation thermography has significant advantages for the detection of large-sized defects in composites such as delamination,[16,17,24] impact damage,[25–27] and foreign object defect (FOD).[24] However, its capability of detecting microsized defects is weak. Flash excited thermography has the capability of detecting porosities in composites, but it does not work for submillimeter porosities.[2,3]

*Address all correspondence to: Hai Zhang, E-mail: hai.zhang.1@ulaval.ca

0091-3286/2016/$25.00 © 2016 SPIE

Downloaded From: https://www.spiedigitallibrary.org/journals/Optical-Engineering on 10/27/2017 Terms of Use: https://spiedigitallibrary.spie.org/ss/TermsOfUse.aspx

Flying spot laser thermography uses a laser that is scanned over the surface. Changes in the heat conductivity then lead to changes in the thermal footprint, which is used for crack detection. This method was suggested for the first time in the late 1960s.[28] A good overview of crack detection with laser excited thermography can be found elsewhere.[29] Rashed et al.[30] first tried to detect cracks with laser excited thermography using modern spatial-resolving IR-cameras. The influences of crack opening and depth to the measurement results were discussed using two-dimensional finite element method (FEM) simulations. Based on this work, a combination of thermography and ultrasound techniques, using the laser for both thermal and acoustical excitation, was suggested.[31,32] Recently, fiber orientation assessment for random preformed CFRP by laser spot thermography was reported.[33,34] However, the detection of submillimeter defects in composites by laser excited thermography was still poorly documented in the open literature.

In addition to optical thermography, ultrasound excited thermography [also known as vibrothermography (VT)] is also increasingly used as an IRT technique in the recently years. This technique utilizes mechanical waves to directly stimulate internal defects without heating the surface as in optical thermography. In classical ultrasound testing, a transducer is placed in contact with the sample with the help of coupling media. The ultrasonic waves travel through the specimen and are transmitted back to the surface where the transducer picks up the reflected signal (pulsed-echo technique), or they are collected on the opposite side (transmission). The principle of defect detection is based on the differences in specific acoustic impedance among materials. In VT, ultrasonic waves travel freely through a homogeneous material, whereas an internal defect produces a complex combination of absorption, scattering, beam spreading, and dispersion of the waves, whose primary manifestation will be in the form of heat. Heat then travels by conduction in all directions; an infrared camera can be directed to one of the surfaces of the specimen to capture the defect signature.[23] Recently the detection of flaws in composites such as delamination, FOD,[35] and cracks[24] has been increasingly reported. However, VT on submillimeter flaws in composites was still poorly documented in the open literature.

In this article, lock-in microlaser line thermography (lock-in micro-LLT) was proposed on the basis of lock-in technique and pulsed microlaser line thermography (pulsed micro-LLT). Microvibrothermography (micro-VT) and microlaser spot thermography (micro-LST) were also proposed by using a microlens. These new techniques were used to investigate the submillimeter porosities in a stitched T-joint CFRP specimen. X-ray microcomputed tomography (micro-CT) was used to validate the thermographic results. Finally, an experimental comparison of microlaser excitation thermography and microultrasonic excitation thermography was conducted.

2 Materials and Methods

2.1 *Specimen*

The T-joint CFRP specimen selected for this evaluation was sewn using stacked TC-06-T 3K carbon fiber. The three-dimensional (3-D) architecture was woven using 3K/12K carbon fiber. A continuous row of stacked 12K tow fiber was used for insertion. A toughened epoxy resin infusion system was selected.[36]

The specimen was fabricated using 3-D preform consisting of multiple layers of woven fabric. The noodle for the T-joint insertion was preshaped through compaction. During processing, the twisted round-shaped stacked 12K carbon fiber tows were placed into the molding tool and compacted to a triangular-shape as the tool was clamped together. After the fiber insertion process was completed, the resin infusion process was initiated.[36]

The complete stitched T-joint CFRP specimen is shown in Fig. 1. The specimen contains six stitching lines. The purpose of the stitching is to consolidate the T-joint structure and to reduce the dry-core. The specimen measures 152 mm in length, 148 mm in width, 63 mm in height, and 5 mm in thickness (excluding the T-stringer). Figure 1(b) shows the detection region.

2.2 *Experimental Configurations*

2.2.1 *Lock-in microlaser line thermography*

A beam expander and a cylindrical lens were reported to convert a laser spot with a radius of around 0.9 mm to a laser line source in the open literature,[37] which is shown in Fig. 2. However, this setup is unsuccessful when using a microlens or microcamera because the distance between the lens and the specimen is only ~4.5 cm. Therefore, the cylindrical lens will block the camera's capture if this setup is used.

The configuration for lock-in micro-LLT in this article is shown in Fig. 3. In the setup, a galvanometer scanning mirror with a frequency of 600 Hz is used to generate the laser line. The position of the laser line can change by modulating the galvanometer scanning mirror, which is shown in Fig. 3(b). Therefore, the setup can avoid blocking the

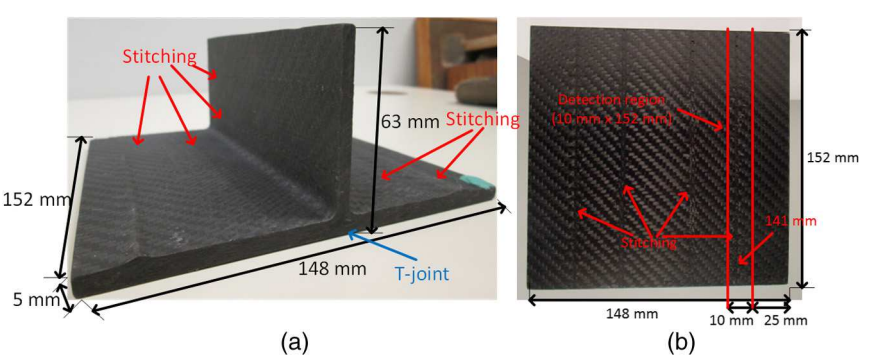

Fig. 1 (a) The complete stitched T-joint CFRP specimen and (b) from flat surface view.

Downloaded From: https://www.spiedigitallibrary.org/journals/Optical-Engineering on 10/27/2017 Terms of Use: https://spiedigitallibrary.spie.org/ss/TermsOfUse.aspx

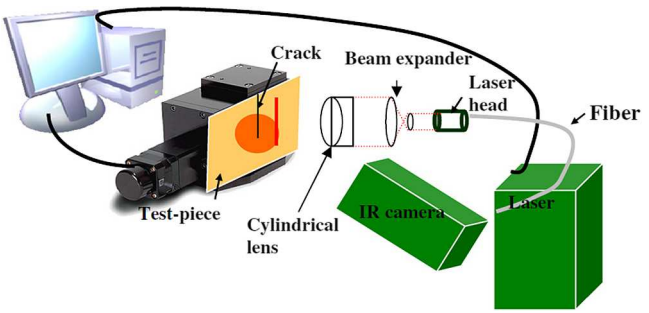

Fig. 2 The laser line thermography setup using a cylindrical lens.[37]

camera's capture, which is more practical for the detection of submillimeter flaws. The laser line is ~13 mm in length and 3 mm in width, and its power is 0.6 W. A microlens with the magnification of 1× is mounted on an infrared camera for identifying and characterizing the submillimeter porosities. The midwave infrared camera "FLIR Phoenix" at a frame rate of 55 fps (640 × 512 pixels) is used to record the temperature profile. The technical specifications of the infrared camera are shown in Table 1. A diode-laser with the wavelength of 805 nm is used as the heating source. A convex lens is used to focus the laser beam. A waveform generator is used to generate the laser line, and another waveform generator is used to generate the lock-in waves (sinusoidal waves). For pulsed micro-LLT, a 0.5-s pulse heating was performed. For lock-in micro-LLT, 1 and 5 Hz lock-in signals heating (20 periods) was conducted on the same zone, respectively here.

2.2.2 *Microlaser spot thermography*

A laser spot was reported to shoot on the specimen directly, and the IR camera was located on the same side of the heating source for laser spot thermography in the open literature.[2,3] However, this setup is not suitable for' instead of submillimeter flaws because the camera is close to the specimen surface when using a microlens or microcamera. This leads to the existence of a laser shooting angle, which will affect the detection results. Therefore, the setup with the galvanometer scanning mirror is also used for micro-LST in this article, which is shown in Fig. 4. The position of the laser spot can change by modulating the mirror angle. A waveform generator is used to generate lock-in waves. The laser spot diameter is 3 mm, and its power is 0.22 W. For pulsed micro-LST, a 0.5-s pulse heating was

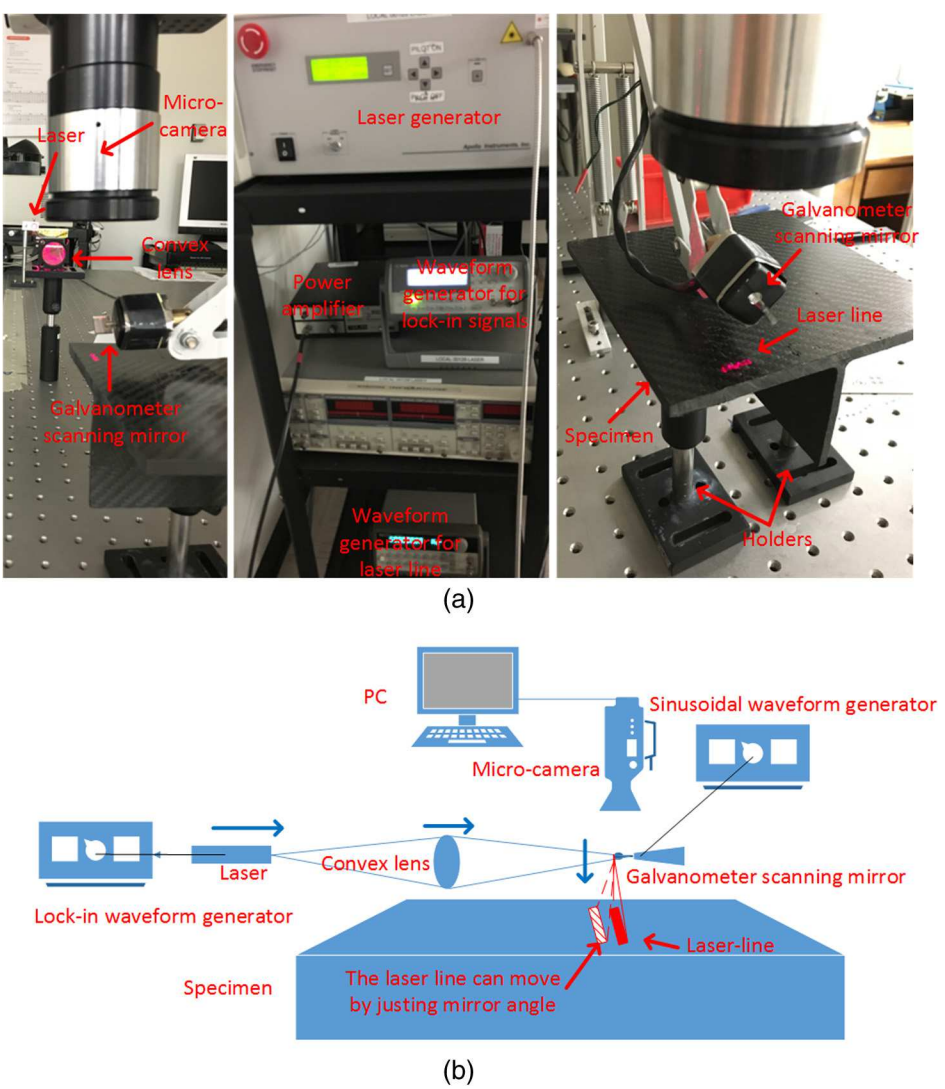

Fig. 3 The lock-in micro-LLT setup: (a) the experimental setup and (b) the schematic setup.

Downloaded From: https://www.spiedigitallibrary.org/journals/Optical-Engineering on 10/27/2017 Terms of Use: https://spiedigitallibrary.spie.org/ss/TermsOfUse.aspx

Table 1 Flir phoenix (MWIR) technical specifications.

Technical specification	Explanation/value
Detector type	Indium antimonide (InSb)
Spectral range	1.5 to 5.0 μm
Cold filter bandpass	3.0 to 5.0 μm standard
Pixel resolution	320 $(H) \times 256\,(V)$ pixels or
	640 $(H) \times 512\,(V)$ pixels
Detector size	30×30 μm for 320×256
	25×25 μm for 640×512
Well capacity	18 M electrons for 320×256
	11 M electrons for 640×512
Integration time	320×256: 9 μs to full frame time
	640×512: <50 μs to full frame time
Sensor assembly $f/\#$	$f/2.5$ standard, $f/4.1$ optional
Sensor cooling	Stirling closed cycle cooler
Spec performance	<25 mK
Max frame rate with DTS electronics	320×256: 345 fps in full frame
	640×512: 100 fps in full frame
Max frame rate with RTIE electronics	320×256: 120 fps in full frame
	640×512: 30 fps in full frame

performed. For lock-in micro-LST, 1 Hz lock-in signal heating (20 periods) was conducted on the same zone.

2.2.3 *Microvibrothermography*

In this article, micro-VT is proposed by using a 1× microlens, which is shown in Fig. 5. The IR camera "Flir Phoenix" with the same configurations as laser thermography is used to record the temperature profile. In the setup, an ultrasound excitation transducer with a pressure of 200 Pa is pressed against the specimen and a burst of ultrasound waves is delivered to the specimen. Table 2 shows the micro-VT generator technical specifications. A 10-s pulsed ultrasound excitation was used. The ultrasound excitation position is located on the back side of the specimen.

2.3 *Infrared Image Processing*

2.3.1 *Cold image subtraction*

Cold image subtraction (CIS) is intended to reduce the effects of fixed artifacts in a thermographic sequence,[38] for example, reflections from the environment such as residual heating coming from the lamps and even the reflection from the camera that appears during the acquisition. Since these artifacts are more or less constant during the whole acquisition, including before heating when the image is cold, this image or the average of several images can be subtracted before heating, so their effect can be reduced.[3] Figure 2 shows an example with an academic aluminum plate.

In Fig. 6, the cold image is affected by noise due to a nonuniform correction (NUC) that was badly performed. This happens when an old NUC is used. The noise can be seen in the raw sequence as well (the second image in Fig. 6), although it is less evident since the temperature is higher.

CIS can be considered as a preprocessing step to improve the quality of the sequence, and then one can use more

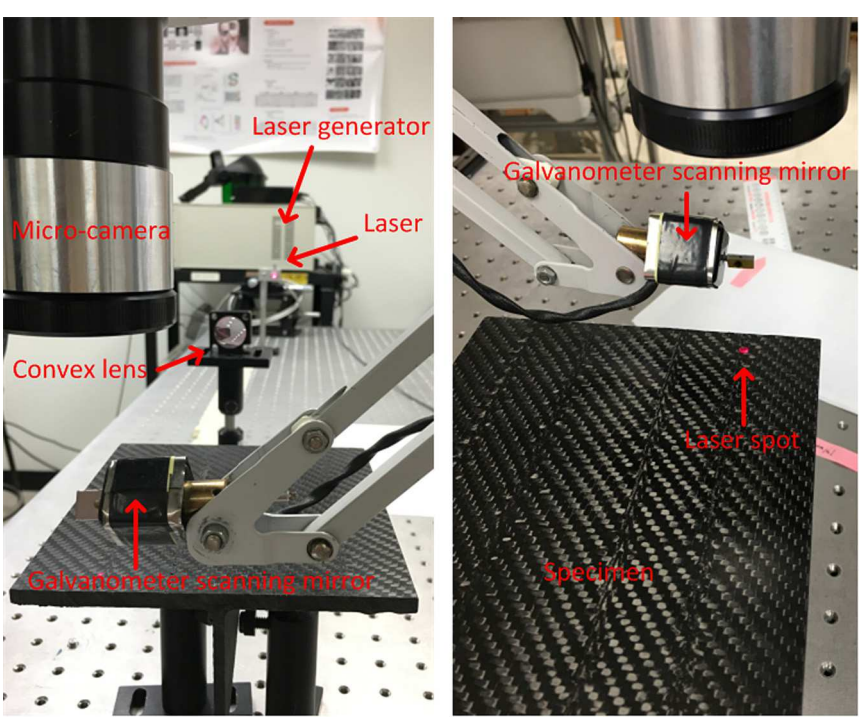

Fig. 4 The micro-LST experimental setup.

Downloaded From: https://www.spiedigitallibrary.org/journals/Optical-Engineering on 10/27/2017 Terms of Use: https://spiedigitallibrary.spie.org/ss/TermsOfUse.aspx

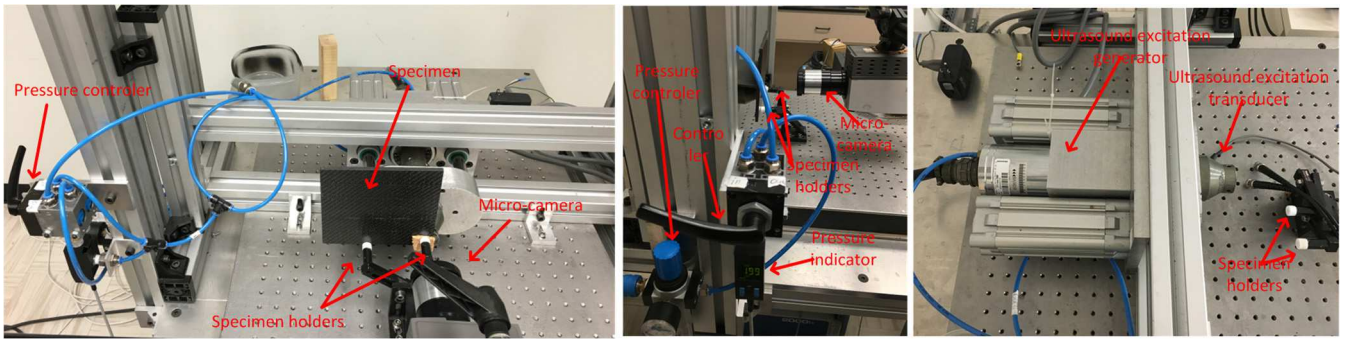

Fig. 5 The micro-VT experimental setup.

Table 2 The microvibrothermography generator technical specifications.

Technical specification	Explanation/value
Ultrasound frequency	15 to 25 kHz
Waveform	Modulation or pulsed
Minimum modulation frequency	0.1 Hz
Maximum excitation time	10 s
Amplitude	0 to 100%

advanced algorithms such as phase pulse thermography and principal component thermography (PCT).

2.3.2 *Principal component thermography*

PCT, originally proposed by Rajic,[39] extracts the image features and reduces undesirable signals. It relies on singular value decomposition, which is a tool to extract spatial and temporal data from a matrix in a compact manner by projecting original data onto a system of orthogonal components known as empirical orthogonal functions (EOF). The first EOF will represent the most important characteristic variability of the data; the second EOF will contain the second most important variability, and so on. Usually, original data can be adequately represented with only a few EOFs. Typically, an infrared sequence of 1000 images can be replaced by 10 or fewer EOFs.[34]

2.3.3 *Lock-in and Fourier transform*

In optical lock-in, the absorption of modulated optical radiation results in a temperature modulation that propagates as a thermal wave into the inspected component. As the thermal wave is reflected at the defect boundary, its superposition to the original thermal wave causes changes in amplitude and phase of the response signal at the surface, which are recorded at the same time using an infrared camera.[40]

From the Fourier's Law one-dimensional solution for a periodic thermal wave propagating through a semi-infinite homogeneous material, the thermal wave diffusion length is given as[41]

$$\mu = \sqrt{\frac{2\alpha}{\omega}} = \sqrt{\frac{\alpha}{\pi f}}, \tag{1}$$

where $\alpha = \kappa/\rho c_p$ is the diffusivity of the material, with κ is the thermal conductivity, ρ is the density, c_p is the specific heat (at constant pressure), and $\omega = 2\pi f$ is the modulation frequency.

The detection depth z is given by the thermal diffusion length equation [42]

$$z = C_1\mu, \tag{2}$$

where C_1 is a correlation constant. The reported values of C_1 range from 1.5 to 2.[42,43]

Generally, inspections start at a relatively high excitation frequency at which, depending on the thermal diffusivity of the material, only shallow defects are visible. In order to detect deeper defects, the excitation frequency is gradually decreased until the appropriate value is reached.

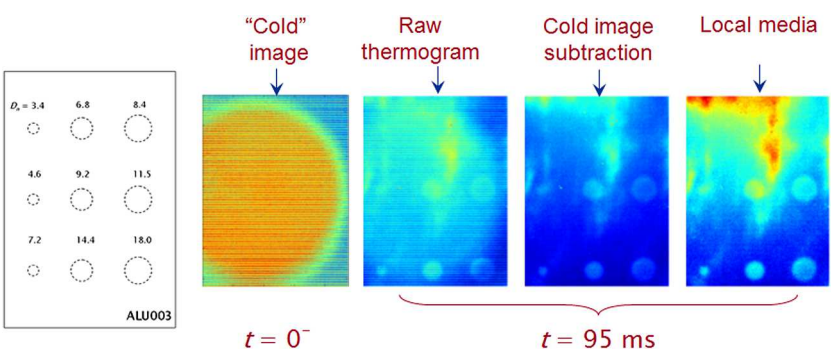

Fig. 6 The example with an academic aluminum plate to explain CIS.

Downloaded From: https://www.spiedigitallibrary.org/journals/Optical-Engineering on 10/27/2017 Terms of Use: https://spiedigitallibrary.spie.org/ss/TermsOfUse.aspx

One commonly used method to retrieve phase and amplitude is four-point methodology for sinusoidal stimulation phase.[44] The four-point methodology is fast but it is valid only for sinusoidal stimulation and is affected by noise. The signal can be denoised in part by averaging several points instead of a single one and/or by increasing the number of cycles. Another possibility is to fit the experimental data using least squares regression[45] and to use this synthetic data to calculate the amplitude and the phase. These two alternatives, however, contribute to slowing down the calculations. Alternatively, the Fourier transform (FT) can be used to extract amplitude and phase information from lock-in data. The FT can be used with any waveform and has the advantage of denoising the signal.[46]

3 Results Analysis

Figure 7 shows micro-CT slices from the position of 141 mm shown in Fig. 1 (b). Figure 7(a) shows the surface of the detected region. Figure 7(b) shows the microporosity A, which appears from the depth of 90 μm. The microporosity A has a diameter of 0.162 mm. Figure 7(c) shows the microporosity B, which appears from the depth of 0.18 mm. The microporosity B has a diameter of 0.216 mm. Figure 7(d) shows the microporosity C, which appears from the depth

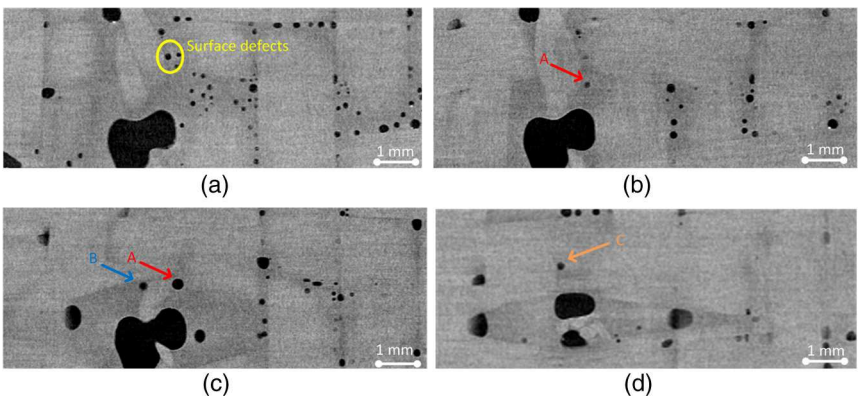

Fig. 7 The micro-CT results (a) surface, (b) depth: 90 μm, (c) depth: 0.18 mm, and (d) depth: 0.414 mm.

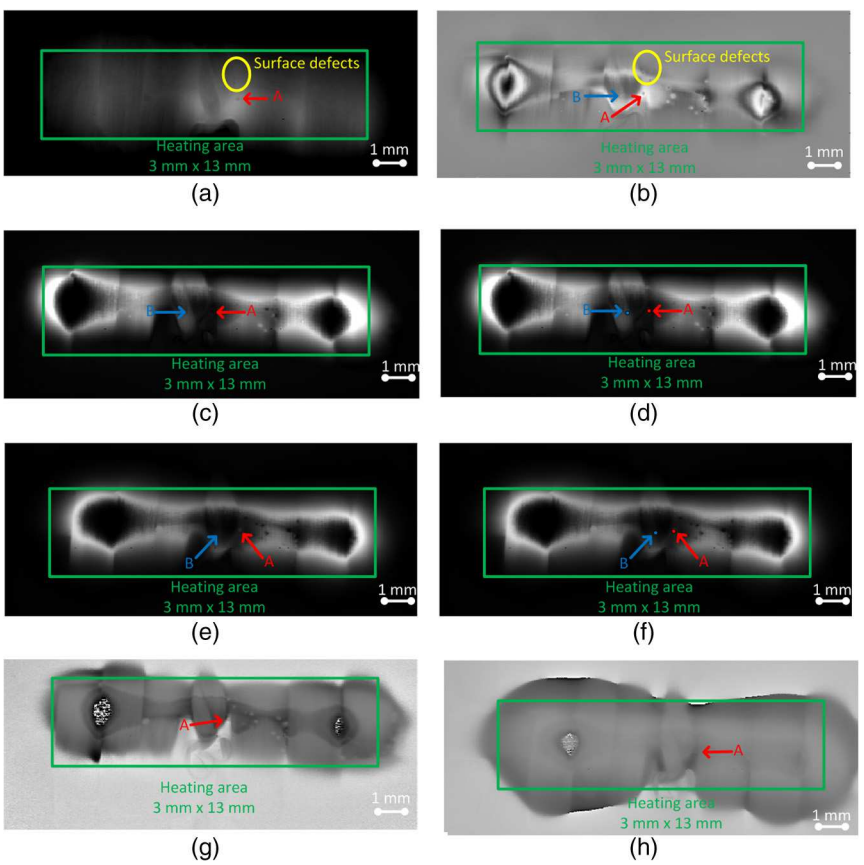

Fig. 8 The micro-LLT results (a) pulse: 0.5 s, cold image, (b) lock-in: 5 Hz, PCT (EOF 8), (c) lock-in: 5 Hz, FT amplitude, (d) lock-in: 5 Hz, FT amplitude (defects marked), (e) lock-in: 1 Hz, FT amplitude, (f) lock-in: 1 Hz, FT amplitude (defects marked), (g) lock-in: 5 Hz, FT phase, and (h) lock-in: 1 Hz, FT phase.

Downloaded From: https://www.spiedigitallibrary.org/journals/Optical-Engineering on 10/27/2017 Terms of Use: https://spiedigitallibrary.spie.org/ss/TermsOfUse.aspx

of 0.414 mm. The microporosity C also has a diameter of 90 μm.

Figure 8 shows the micro-LLT results. Figure 8(a) shows the pulsed micro-LLT result after CIS when the heating source is a 0.5-s pulse. The microporosity A can be detected. In lock-in method, the microporosity B cannot be detected in the raw images as in the pulse method. However, the images after image processing can provide more defect information. Figure 8(b) shows the lock-in result after PCT. The microporosity A can be detected in the image. The microporosity B is also detected, but not as clearly as the microporosity A. Figures 8(c) and 8(e) show the lock-in results after FT on amplitude. The microporosities A and B can be detected, but not clearly. The microporosity A is clearer when the lock-in frequency is 1 Hz. On the contrary, the microporosity B is clearer when the lock-in frequency is 5 Hz. The positions of the microporosities A and B are correspondingly marked in Figs. 8(d) and 8(f). Figures 8(g) and 8(h) show the lock-in results after FT on phase. The microporosity A can be detected, but not clearly. The microporosity B cannot be detected as in the amplitude case.

Figure 9 shows the micro-LST results. Figure 9(a) shows the 0.5-s pulse laser heating result after CIS. The microporosity A is detected. The microporosity B cannot be inspected by any image processing methods, similar to the corresponding pulsed micro-LLT results. As in the lock-in micro-LLT results, the microporosity B cannot be detected in the raw images, but can be detected in postprocessing images. Figure 9(b) shows the lock-in result after PCT. The positions of the microporosities A and B are anomalous.

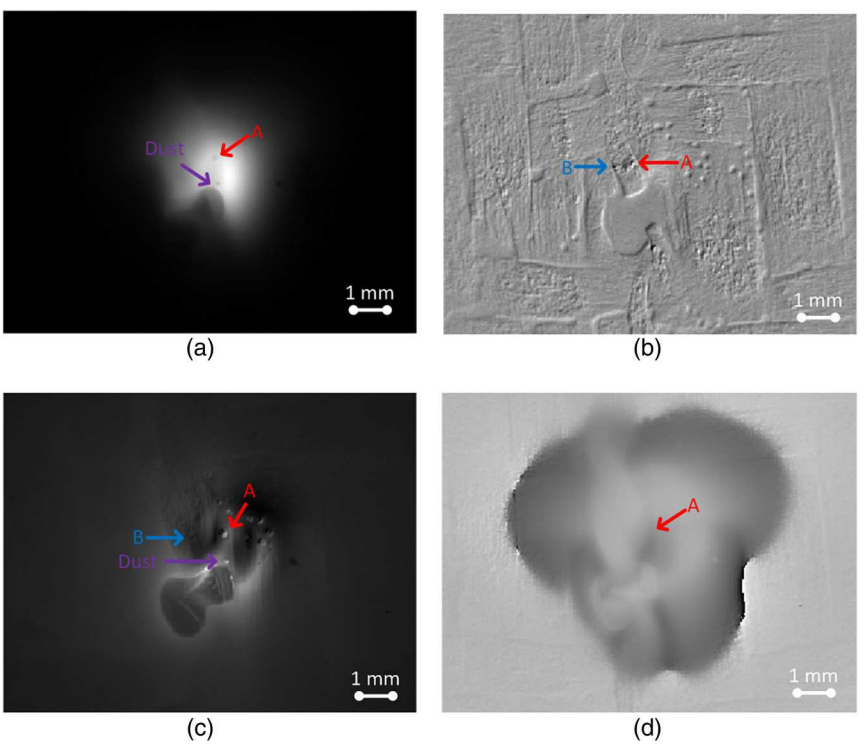

Fig. 9 The micro-LST results (a) pulse: 0.5 s, cold image, (b) lock-in: 1 Hz, PCT (EOF 5), (c) lock-in: 1 Hz, FT amplitude, and (d) lock-in: 1 Hz, FT phase.

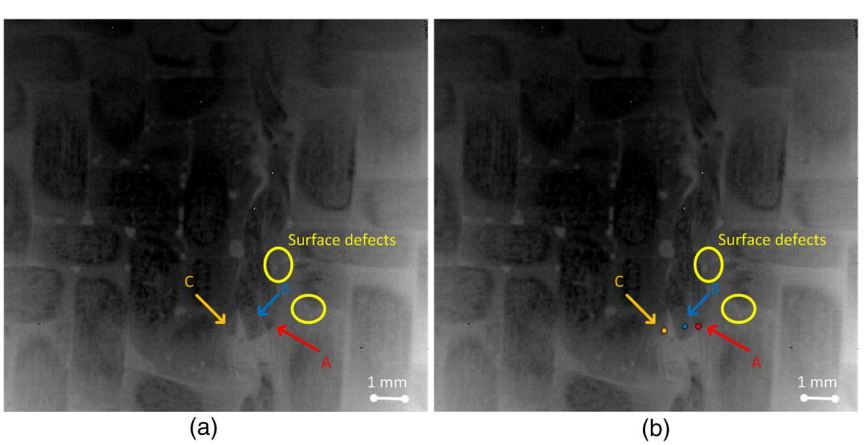

Fig. 10 The micro-VT results (a) pulse: 10 s and (b) pulse: 10 s (defects marked).

Downloaded From: https://www.spiedigitallibrary.org/journals/Optical-Engineering on 10/27/2017 Terms of Use: https://spiedigitallibrary.spie.org/ss/TermsOfUse.aspx

Table 3 The experimental thermographic results.

Submillimeter porosity	Pulsed micro-LLT and LST			Lock-in micro-LLT and LST				Micro-VT
Depth	Raw image	CIS	PCT	Raw image	PCT	FT on phase	FT on amplitude	Raw image
Surface	1	1	1	1	1	1	1	1
90 μm	1	1	1	1	1	1	1	1
180 μm	0	0	0	0	1	0	1	1
414 μm	0	0	0	0	0	0	0	1

One can conclude that the microporosities A and B are detected in this image. However, this result is not absolutely reliable. Figure 9(c) shows the lock-in result after FT on amplitude. The microporosities A and B are detected clearly. The microporosity A is clearer than the microporosity B. Compared to the corresponding laser line method, the microporosity B is clearer. Figure 9(d) shows the lock-in result after FT on phase. Similar to the corresponding laser line results, the microporosity A can be detected, but not clearly. The microporosity B cannot be detected.

Figure 10 shows the corresponding micro-VT results. Figure 10(a) shows the micro-VT result, which is from the raw images. The postprocessing images do not provide better results. Compared to the micro-CT slices, microporosities on the surface can be detected. The microporosities A, B, and C can also be detected, but not clearly. The three microporosities are marked in Fig. 10(b). The microporosities A, B, and C show a similar size and shape, which is absolutely wrong.

Table 3 shows the experimental thermographic results, where "1" indicates that the corresponding porosity is found, and "0" indicates that the corresponding porosity is not found. As a conclusion, the lock-in technique can detect a deeper depth than the pulsed technique. However, the clarity of the results decreases rapidly as the detection depth increases in PCT results. The amplitude FT results can provide more information than phase calculation. The FT results are not as clear as the CIS results, but CIS is not suitable for the lock-in technique. The laser spot method is more powerful than the corresponding laser line method even if the laser spot power is lower compared to the laser line power. Micro-VT can detect a larger zone and deeper depth than laser excitation thermography, but the detection size and shape information is not accurate.

4 Conclusion

In this article, IRT approaches including micro-VT, micro-LLT, and micro-LST on the basis of lock-in and pulsed techniques were proposed. These approaches were used to detect the submillimeter porosities in a stitched T-joint CFRP specimen. Micro-CT was used to validate the thermographic results. Finally an experimental comparison of microlaser excitation thermography and microultrasonic excitation thermography was conducted. As a conclusion, micro-VT can provide the deepest detection depth, but the size and shape information is not accurate. The lock-in technique can identify a deeper depth than the pulsed technique. The laser spot method can provide clearer results than the laser line method, but is not practical due to the limitation of detection zone.

For laser excitation thermography, a potential way to enhance the maximum detection depth is to increase the laser power, but there is a risk that the CFRP specimen would be damaged. Another potential way is to use lower lock-in frequencies, which need massive experiments. An FEM is beneficial to the analysis of the lock-in technique,[47,48] especially by using infrared image processing techniques. This may greatly reduce the quantity of experiments and predict the thermographic results. A robotic detection technique can also reduce the duration of the experiments and improve the detection efficiency, which will require the corresponding image reconstruction algorithms.[49]

Acknowledgments

This research was supported by the Consortium for Research and Innovation in Aerospace in Québec (CRIAQ) through Project No. CRIAQ COMP-501 - CRDPJ 408010-10. This research was also supported by the governments of Québec and Bavaria, Ministère des Relations Internationales and Ministry of External Affairs through bilateral Project No. 13.311. The authors would like to acknowledge the support provided by the Natural Sciences and Engineering Research Council of Canada (NSERC) and the industrial partners: Bell Helicopter (Canada) Inc., Bombardier Inc Hutchinson Inc., Delastek Inc., Texonic Inc., and CTT group. The authors would also like to thank Wolfgang Holub from Fraunhofer EZRT (Germany) for his assistance and the funding provided by the Brazilian National Council for Scientific and Technological Development -CNPq (Process 166285/2015-3).

References

1. T. J. Kang and S. H. Lee, "Effect of stitching on the mechanical and impact properties of woven laminate composite," *J. Compos. Mater.* **28**(16), 1574–1587 (1994).
2. H. Zhang et al., "Infrared thermography, ultrasound c-scan and microscope for non-destructive and destructive evaluation of 3D carbon fiber materials: a comparative study," *Proc. SPIE* **9485**, 94850X (2015).
3. H. Zhang et al., "Comparative study on submillimeter flaws in stitched t-joint carbon fiber reinforced polymer by infrared thermography, microcomputed tomography, ultrasonic c-scan and microscopic inspection," *Opt. Eng.* **54**(10), 104109 (2015).
4. B. Liu et al., "Weak magnetic flux leakage: a possible method for studying pipeline defects located either inside or outside the structures," *NDT & E Int.* **74**, 81–86 (2015).
5. B. Liu et al., "Study on characteristics of magnetic memory testing signal on the stress concentration field," *IET Sci., Meas. Technol.* (2016).
6. Y. Bar-Cohen, "Emerging NDT technologies and challenges at the beginning of the third millennium, part 2," *Mater. Eval.* **58**(2), 141–150 (2000).
7. S. Sfarra et al., "Non-destructive testing techniques to help the restoration of frescoes," *Arabian J. Sci. Eng.* **39**(5), 3461–3480 (2014).
8. S. Sfarra et al., "Diagnostics of wall paintings: a smart and reliable approach," *J. Cult. Heritage* **18**, 229–241 (2016).

Downloaded From: https://www.spiedigitallibrary.org/journals/Optical-Engineering on 10/27/2017 Terms of Use: https://spiedigitallibrary.spie.org/ss/TermsOfUse.aspx

9. S. Sfarra et al., "Holographic interferometry (HI), infrared vision and x-ray fluorescence (XRF) spectroscopy for the assessment of painted wooden statues: a new integrated approach," *Appl. Phys. A* **115**(3), 1041–1056 (2014).
10. S. Sfarra et al., "Santa maria di collemaggio church (L'aquila, Italy): historical reconstruction by non-destructive testing techniques," *Int. J. Archit. Heritage* **9**(4), 367–390 (2015).
11. S. Sfarra et al., "How to retrieve information inherent to old restorations made on frescoes of particular artistic value using infrared vision?" *Int. J. Thermophys.* **36**(10–11), 3051–3070 (2015).
12. S. Sfarra et al., "Discovering the defects in paintings using non-destructive testing (NDT) techniques and passing through measurements of deformation," *J. Nondestr. Eval.* **33**(3), 358–383 (2014).
13. S. Sfarra et al., "Evaluation of defects in panel paintings using infrared, optical and ultrasonic techniques," *Insight* **54**(1), 21–27 (2012).
14. S. Sfarra et al., "Integrated approach between pulsed thermography, near-infrared reflectography and sandwich holography for wooden panel paintings advanced monitoring," *Russ. J. Nondestr. Test.* **47**(4), 284–293 (2011).
15. M. Tortora et al., "Non-destructive and micro-invasive testing techniques for characterizing materials, structures and restoration problems in mural paintings," *Appl. Surf. Sci.* **387**, 971–985 (2016).
16. S. Sfarra et al., "Monitoring of jute/hemp fiber hybrid laminates by nondestructive testing techniques," *Sci. Eng. Compos. Mater.* **23**(3), 283–300 (2016).
17. S. Sfarra et al., "Eco-friendly laminates: from the indentation to non-destructive evaluation by optical and infrared monitoring techniques," *Strain* **49**(2), 175–189 (2013).
18. B. Yousefi et al., "Mineral identification in hyperspectral imaging using Sparse-PCA," *Proc. SPIE* **9861**, 986118 (2016).
19. B. Yousefi et al., "Emissivity retrieval from indoor hyperspectral imaging of mineral grains," *Proc. SPIE* **9861**, 98611C (2016).
20. S. Sfarra et al., "Thermographic, ultrasonic and optical methods: a new dimension in veneered wood diagnostics," *Russ. J. Nondestr. Test.* **49**(4), 234–250 (2013).
21. S. Sfarra et al., "Ceramics and defects," *J. Therm. Anal. Calorim.* **123**(1), 43–62 (2016).
22. X. Maldague, *Theory and Practice of Infrared Technology for Nondestructive Testing*, Wiley, New York (2001).
23. C. Ibarra-Castanedo and X. P. Maldague, "Infrared thermography," in *Handbook of Technical Diagnostics*, pp. 175–220, Springer, New York (2013).
24. B. Liu et al., "Quantitative evaluation of pulsed thermography, lock-in thermography and vibrothermography on foreign object defect (FOD) in CFRP," *Sensors* **16**(5), 743 (2016).
25. S. Sfarra et al., "An innovative nondestructive perspective for the prediction of the effect of environmental aging on impacted composite materials," *Int. J. Eng. Sci.* **102**, 55–76 (2016).
26. A. Bendada et al., "How to reveal subsurface defects in Kevlar® composite materials after an impact loading using infrared vision and optical NDT techniques?," *Eng. Fract. Mech.* **108**, 195–208 (2013).
27. S. Sfarra et al., "Falling weight impacted glass and basalt fibre woven composites inspected using non-destructive techniques," *Compos. Part B: Eng.* **45**(1), 601–608 (2013).
28. E. J. Kubiak, "Infrared detection of fatigue cracks and other near-surface defects," *Appl. Opt.* **7**(9), 1743–1747 (1968).
29. C. Gruss, F. Lepoutre, and D. Balageas, "Nondestructive evaluation using a flying-spot camera," *ONERA TP* **1** (1993).
30. A. Rashed et al., "Crack detection by laser spot imaging thermography," in *AIP Conf. Proc.*, Vol. **894**(1), 500–506 (2007).
31. S. E. Burrows et al., "Combined laser spot imaging thermography and ultrasonic measurements for crack detection," *Nondestr. Test. Eval.* **22**(2-3), 217–227 (2007).
32. J. Schlichting, C. Maierhofer, and M. Kreutzbruck, "Crack sizing by laser excited thermography," *NDT & E Int.* **45**(1), 133–140 (2012).
33. H. Fernandes, H. Zhang, and X. Maldague, "An active infrared thermography method for fiber orientation assessment of fiber-reinforced composite materials," *Infrared Phys. Technol.* **72**, 286–292 (2015).
34. H. Fernandes et al., "Fiber orientation assessment on randomly-oriented strand composites by means of infrared thermography," *Compos. Sci. Technol.* **121**, 25–33 (2015).
35. H. Fernandes et al., "Thermographic non-destructive evaluation of carbon fiber-reinforced polymer plates after tensile testing," *J. Nondestr. Eval.* **34**(4), 1–10 (2015).
36. H. Zhang et al., "An experimental and analytical study of micro-laser line thermography on micro-sized flaws in stitched carbon fiber reinforced polymer composites," *Compos. Sci. Technol.* **126**, 17–26 (2016).
37. T. Li, D. P. Almond, and D. A. S. Rees, "Crack imaging by scanning laser-line thermography and laser-spot thermography," *Meas. Sci. Technol.* **22**(3), 035701 (2011).
38. C. Alard and R. H. Lupton, "A method for optimal image subtraction," *Astrophys. J.* **503**(1), 325 (1998).
39. N. Rajic, "Principal component thermography for flaw contrast enhancement and flaw depth characterisation in composite structures," *Compos. Struct.* **58**(4), 521–528 (2002).
40. A. Gleiter, C. Spießberger, and G. Busse, "Lockin thermography with optical or ultrasound excitation," *Strojniški Vestn.-J. Mech. Eng.* **56**(10), 619–624 (2010).
41. G. Giorleo and C. Meola, "Comparison between pulsed and modulated thermography in glass–epoxy laminates," *NDT & E Int.* **35**(5), 287–292 (2002).
42. G. Busse and A. Rosencwaig, "Subsurface imaging with photoacoustics," *Appl. Phys. Lett.* **36**, 815 (1980).
43. R. Thomas et al., "Subsurface flaw detection in metals by photoacoustic microscopya," *J. Appl. Phys.* **51**(2), 1152–1156 (1980).
44. G. Busse, D. Wu, and W. Karpen, "Thermal wave imaging with phase sensitive modulated thermography," *J. Appl. Phys.* **71**(8), 3962–3965 (1992).
45. J. Krapez, "Compared performances of four algorithms used for modulation thermography," in *Proc. of the Eurotherm Seminar*, Vol. 60, pp. 7–10 (1998).
46. Y. Duan et al., "Quantitative evaluation of optical lock-in and pulsed thermography for aluminum foam material," *Infrared Phys. Technol.* **60**, 275–280 (2013).
47. H. Zhang et al., "A comparative study of experimental and finite element analysis on submillimeter flaws by laser and ultrasonic excited thermography," *Proc. SPIE* **9861**, 98611A (2016).
48. H. C. Fernandes et al., "Infrared thermography for CFRP inspection: computational model and experimental results," *Proc. SPIE* **9861**, 98610H (2016).
49. B. Yousefi et al., "Hierarchical segmentation of urban satellite imagery," *Int. J. Appl. Earth Obs. Geoinf.* **30**, 158–166 (2014).

Hai Zhang works in the Computer Vision and Systems Laboratory (CVSL), Department of Electrical and Computer Engineering, Laval University, Canada. He was also a visiting researcher in the Fraunhofer Development Center X-ray Technologies (EZRT), Fraunhofer IIS, Fuerth, Germany. He is the author of more than 20 publications. His research interests include vision and digital systems for industrial inspection, additive manufacturing and nondestructive evaluation (NDE) via infrared thermography, x-ray computed tomography, ultrasonic c-scan, and terahertz imaging.

Xavier Maldague has been a full professor in the Department of Electrical and Computing Engineering, Laval University, Quebec City, Canada, since 1989, head of the Department from 2003 to 2008. He has trained over 50 graduate students (MSc and PhD) and has more than 300 publications. His research interests are infrared thermography, nondestructive evaluation (NDE) techniques, and vision/digital systems for industrial inspection. He holds a tier 1 Canada research chair in infrared vision.

Biographies for the other authors are not available.

Downloaded From: https://www.spiedigitallibrary.org/journals/Optical-Engineering on 10/27/2017 Terms of Use: https://spiedigitallibrary.spie.org/ss/TermsOfUse.aspx